# Algorithm Theoretical Basis Document

# MERIS L2 Algorithm for Total Column Water Vapour

Issue 1 Revision 1

Institute for Space Sciences,

Freie Universität Berlin

14 December 2014

## Document Change Record

| Document, Version | Date | Changes | Originator |
|---|---|---|---|
| DOC, v1.0 | 2012.11.16 | Original version,<br>addapted from GlobVapour_D07_ATBD_L2_MERIS_v3.0.doc | Hannes Diedrich<br>(Rasmus Lindstrot) |
| DOC, v1.1 | 2014.14.14 | • Windspeed now from ECMWF<br>• Estimation of surface albedo ratio uncertainty only for $\rho>0.05$ | Rene Preusker |

# Table of Contents

# 1 Introduction

## 1.1 Purpose

This document provides the Algorithm Theoretical Basis of the Level 2 MERIS total column water vapour product.

## 1.2 Definitions, acronyms and abbreviations

| | |
|---|---|
| AOT | Aerosol Optical Thickness |
| DOAS | Differential Optical Absorption Spectroscopy |
| MERIS | Medium Resolution Imaging Spectrometer |
| MOMO | Matrix Operator Model |
| NDVI | Normalized Differenced Vegetation Index |
| SSM/I | Special Sensor Microwave Imager |
| TCWV | Total Columnar Water Vapour |
| FUB | Freie Universität Berlin |

## 1.3 Reference Documents


[RD-1] Bennartz, R. and Fischer, J., 2001. Retrieval of columnar water vapour over land from backscattered solar radiation using the Medium Resolution Imaging Spectrometer, Remote Sensing of Environment, 78, 274-283, DOI: 10.1016/S0034-4257(01)00218-8.

[RD-2] Fischer, J. and Bennartz, R., 1997. Retrieval of total water vapor content from MERIS measurements. Algorithm Theoretical Basis Document PO-NT-MEL-GS-005, ESA-ESTEC.

[RD-3] Leinweber, R. and Fischer, J., 2010, Water vapor retrieval from MERIS satellite measurements over cloud free land surfaces, submitted to Journal of Applied Meteorology and Climatology.

[RD-4] Rothman, L.S. and coauthors, 2009, The HITRAN 2008 molecular spectroscopic database, Journal of Quantitative Spectroscopy & Radiative Transfer 110, 533–572.

[RD-5] DUE GLOBVAPOUR Metadata Definition, issue 1, revision 2, dated 07 September 2010

[RD-6] Fischer, J. (1988). High-resolution spectroscopy for remote sensing of physical cloud properties and water vapour. In: J. Lenoble, & J.-F. Geleyn (Eds.), Current problems in atmospheric radiation (pp. 151–156). Hampton, Virginia, USA: Deepak Publishing.

[RD-7] Fischer, J. and Grassl, H., 1984, Radiative transfer in an atmosphere—ocean system: an azimuthally dependent matrix-operator approach, Applied Optics 23 (7), 1032-1039 (1984), doi:10.1364/AO.23.001032

[RD-8] Fell, F., and Fischer, J., 2001, Numerical simulation of the light field in the atmosphere-ocean system using the matrix-operator method, Journal of Quantitative Spectroscopy & Radiative Transfer 69, 351-388.

[RD-9] McClatchey, R., R. Fenn, J. Selby, F. Volz, and J. Garing, 1972: Optical Properties of the Atmosphere. Air Force Cambridge Research Laboratories, 3rd edition.

[RD-10] Bennartz, R., and J. Fischer, 2000, A modified k-distribution approach applied to narrow band water vapor and oxygen absorption estimates in the near infrared JQSRT, 66, 539-553

[RD-11] Fischer, J. ; Preusker, R.; Muller, J.-P. & M. Zühlke, 2007: ALBEDOMAP -Validation Report - ESA AO/1-4559/04/I-LG, Online-Publikation: http://www.brockmann-consult.de/albedomap/pdf/MERIS-AlbedoMap-Validation-1.0.pdf.

[RD-12] Cox, C. and Munk, W., 1954: Measurement of the Roughness of the Sea Surface from Photographs of the Sun's Glitter, J. Opt. Soc. Am., 44, 838-850, doi:10.1364/JOSA.44.000838

[RD-13] Delwart, S.; Preusker, R.; Bourg, L.; Santer, R.; Ramon, D. & Fischer, J., 2007, MERIS inflight spectral calibration, Int. J. Rem. Sens., 28, 479 - 496.

[RD-14] Lindstrot, R.; Preusker, R. & Fischer, J., 2010, The empirical correction of stray light in the MERIS oxygen A band channel J. Atmos. Oceanic Technol., 27, 1185-1194

[RD-15] Rodgers, C., 2000, Inverse Methods for Atmospheric Sounding: Theory and Practice *World Scientific, London*

[RD-16] Koepke, P., Effective reflectance of oceanic whitecaps, 1984**,** Appl. Opt., 23, 1816–1824.

[RD-17] Ptashnik, I. V.; Shine, K. P. & Vigasin, A. A., 2011, Water vapour self-continuum and water dimers: 1. Analysis of recent work, Journal of Quantitative Spectroscopy & Radiative Transfer, 112, 1286–1303.

[RD-18] Lindstrot, R., Preusker, R., Diedrich, H., Doppler, L., Bennartz, R., and Fischer, J., 2012: 1-D-Var retrieval of daytime total columnar water vapour from MERIS measurements, Atmos. Meas. Tech., 5, 631-646, doi:10.5194/amt-5-631-2012

[RD-19] Breon, F.M., An analytical model for the cloud-free atmosphere/ocean system reflectance, Remote Sensing of Environment (ISSN 0034-4257), vol. 43, no. 2, p. 179-192.

## 1.4 Structure of the document

Section 2 gives an overview of the MERIS instrument and the retrieval algorithm scheme. The used methods, models and preparatory works are introduced. In section 3 both the theoretical basis of the algorithm as well as the practical application are detailed. Necessary assumptions and limitations are described in section 4. Section 5 gives a conclusion.

# 2 Algorithm overview

## 2.1 Water vapour over land surfaces

The algorithm for the retrieval of TCWV from measurements of MERIS is based on the exploitation of the pronounced water vapour absorption band around 950 nm using the differential absorption of water vapour. A similar approach was described by, e.g., Bennartz and Fischer (2001) ([RD-1]) and implemented in the MERIS ground segment ([RD-2]; [RD-3]).

MERIS is a wide field-of-view imaging pushbroom spectrometer, providing measurements in 15 spectral channels between 400 nm and 900 nm. The spatial resolution in the reduced resolution mode is 1 x 1 $km^2$ and the swath width is roughly 1150 km. MERIS is one out of ten core instruments on ENVISAT and therefore provides continuous observations since March 2002. ENVISAT is flying in a sun-synchronous orbit, descending node, with a constant equator crossing time of 10 LT.

The full MERIS spectrum is used in the retrieval scheme, whereupon the majority of the spectral bands are exploited for cloud screening. Ultimately, three spectral channels are used for the retrieval of water vapour: Channels 13 and 14, located at 865 nm and 885 nm, respectively, provide measurements in the atmospheric window region whereas channel 15, located at 900 nm, at the shortwave edge of the $\varphi\phi\tau$-absorption band, is strongly influenced by atmospheric water vapour. Here the ratio of MERIS bands 15 and 14 is used for the approximation of the atmospheric transmittance in the water vapour absorption band which is closely related to the total column amount. In order to avoid errors due to the spectral variation of the surface reflectivity between 885nm and 900nm, MERIS band 13 is additionally used for the linear extrapolation of the surface reflectivity from MERIS bands 13 and 14 to 15.

The algorithm does not rely on auxiliary data except for monthly MODIS snow masks and information about the aerosol optical thickness that is available from e.g. MERIS L2 data. However, due to the weak influence of the aerosol scattering over the relatively bright land, the retrieval is not essentially hampered if a climatological mean value of aerosol optical thickness (AOT) is used. In a first step, the MERIS L1B data is screened for clouds, using an Artificial Neural Network developed at FUB. In the next step, the surface reflectance at 865 nm and 885 nm is derived from MERIS L1B data, assuming a Lambertian surface and single scattering conditions. The surface reflectance at 900 nm is then inferred from a linear extrapolation of the window channel reflectances. The gaseous absorption coefficients, based on HITRAN 2008 data ([RD-4]) and pre-calculated using an advanced k-distribution routine from [RD-1], are chosen according to the most appropriate temperature profile, depending on latitude and season. The channel ratio *R* of MERIS bands 15 and 14 is modelled by

1. calculating the transmittance at 900 and 885nm for a given water vapour amount and observation geometry and
2. applying a scattering correction to the modelled transmittance ratio, depending on the observation geometry, the surface reflectance, AOT and the water vapour amount itself.

The total columnar water vapour (TCWV) is inferred by matching the channel ratio *R* with the modelled channel ratio using the secant method.

Due to the strong water vapour sensitivity of the MERIS measurements, the algorithm does not rely on prior knowledge and background information such as water vapour from ERA Interim reanalyses. Reliable aerosol information is beneficial but not crucial.

Realistic uncertainty estimates are provided by taking into account all relevant sources of error such as sensor noise, and errors of forward modelling parameters such as AOT, aerosol vertical distribution, surface reflectance, surface elevation and temperature.
Figure 1 shows a flow chart of the MERIS L2 algorithm for the retrieval of TCWV.

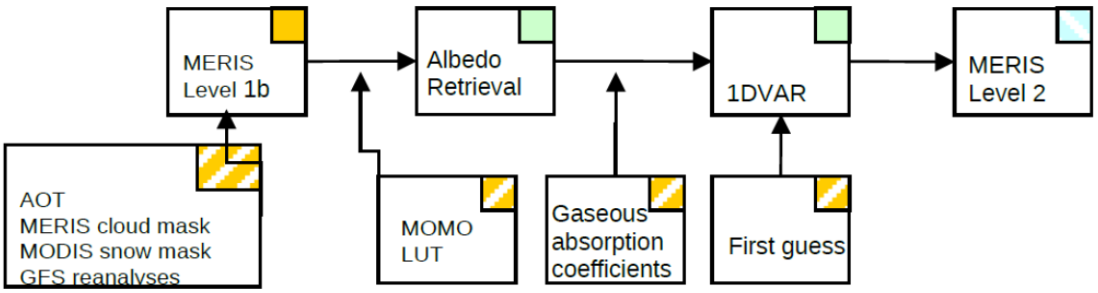


**Figure 1: Flow chart for the MERIS L2 processor. Input data is marked in orange (orange shaded: higher level input data), products are marked in blue (blue shaded: instantaneous level 2 products) and software development is marked in green. (GFS: Global Forecasting System, LUT: Look-up table)**

The resulting MERIS L2 data are stored in NetCDF files that are fully compliant with the NetCDF Climate Forecast convention. A detailed description of the output file format can be found in [RD-5].

## 2.2 Water vapour over ocean surfaces

The ocean-surface component of the MERIS L2 processor has been improved. The inversion scheme is identical with the one over land, only the scattering correction is different. For this reason, radiative transfer simulations were performed for a dark ocean surface. The surface reflectance of the ocean depends amongst others (viewing geometry, salinity...) on the wind-speed [RD-12]. Thus, the lower boundary condition over the ocean is the wind-speed as parametrization of the sea surface roughness, rather than the surface albedo. The results were stored in look-up-tables.

Additionally the determination of the scattering factor distinguishes between surfaces with high (glint area) and low surface reflectance (off-glint area).

Figure 2 shows a flow chart of the MERIS L2 algorithm for the retrieval of TCWV over the ocean.

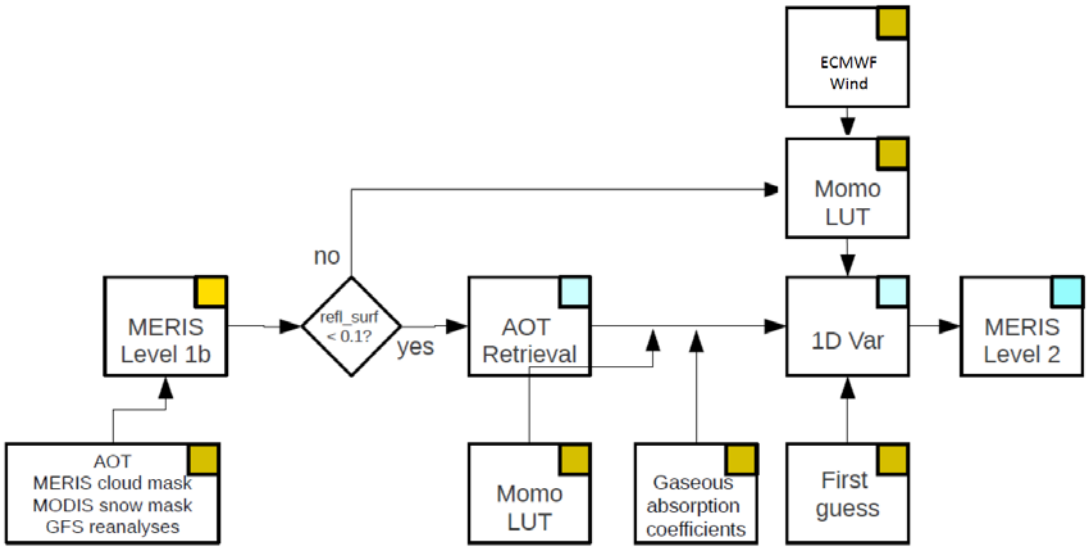


Figure 2: Flow chart for the MERIS L2 processor the ocean surfaces. Input data is marked in orange (dark-orange : higher level input data), products are marked in blue. (GFS: Global Forecasting System, LUT: Look-up table)

# 3 Algorithm description

## 3.1 Theoretical description

The absorption of electromagnetic radiation by water vapour, occurring at characteristic wavelengths throughout the solar and terrestrial spectrum, is related to the excitation of various combinations of the three fundamental vibrational modes of the water molecule. Measurements of the reflected sun light within the resulting absorption bands enable a determination of TCWV, provided that

1. incoming solar radiation is available, precluding night-time retrievals,
2. the channel used is located in a non-saturated and therefore sufficiently sensitive part of the absorption band,
3. the optical thickness of other atmospheric species is either zero or precisely known,
4. the surface albedo is known or can be accurately estimated,
5. the paths of the detected photons through the atmosphere are either known to a sufficient degree or predominantly attributable to the non-scattered, surface-reflected fraction,
6. the lower troposphere, holding the main part of TCWV, is not obscured by clouds or optically thick aerosol layers.

For monochromatic radiation, the transmittance $T$ through a medium can be related to its optical depth $\tau$ and the air mass $\mu$, following the Beer-Lambert law:

$$T = exp(-\tau/\mu)$$

Neglecting scattering processes and assuming non-saturated absorption, the mass of the absorbing species can thus be directly related to the logarithm of the traversed medium's transmittance. Since the transmittance cannot be measured directly from space, it has to be approximated by the ratio of two neighbouring bands with differing optical depth. Fischer ([RD-6]) proposed to use two closely spaced bands, with one channel located in the in the shortwave end of the $\rho\sigma\tau$-absorption band around 900nm and the other one in the atmospheric window region around 885nm. At this spectral range, almost all land surfaces such as vegetated, bare soil or snow-covered areas, are bright and therefore provide a good background for retrievals of total columnar amounts of water vapour. The small spectral distance of merely 15nm minimizes the difference in surface reflectance and atmospheric scattering properties between the two bands. Finally, by locating the absorption channel at 900nm instead of sensing higher optical depths of water vapour at e.g. 950nm, it is assured that the measurements are sensitive to TCWV throughout the range of globally occurring water vapour column amounts. This is due to the fact that the water vapour absorption at 900nm does not get saturated, even in case of high air masses in a humid atmosphere. Therefore, the MERIS bands are perfectly suited for the daytime, cloud-free retrieval of TCWV over land.
Around 900nm, the ocean surface is dark, except for observing geometries featuring direct, specular reflection of sun light. One therefore has to accept a reduced accuracy of the derived TCWV over ocean due to the stronger impact of the uncertain atmospheric scattering on the measured band ratio.

## 3.2 Practical application

Since the retrieval algorithm is required to provide

1. flexibility regarding the inclusion of auxiliary information such as background knowledge about aerosol loading and the surface temperature and
2. uncertainty estimates on a pixel-by-pixel basis,

the inversion of the MERIS measurements is carried out by one-dimensional variational analysis (1D-Var), instead of relying on e.g. non-linear regression approaches such as artificial neural networks. The drawback of this solution is a considerable increase in computing time, necessitating a fast forward simulation module.
The retrieval scheme is divided into several individual steps, starting with a determination of the surface reflectance in MERIS bands 14 and 15 and a subsequent iterative optimization of TCWV by minimizing the cost function, represented by the absolute difference between the modelled and observed ratios of MERIS bands 15 and 14. In order to account for the influence of scattering on the measured water vapour transmittance, a scattering correction factor is calculated at each retrieval step, depending on surface reflectance (in case of an ocean surface depending on the wind speed), viewing geometry, AOT and TCWV itself. The uncertainty of the retrieved value of TCWV is calculated after the final iteration step, by taking into account uncertainties introduced by instrumental effects such as sensor noise and uncertainties in prior knowledge of the influencing parameters such as surface albedo, aerosol optical depth, aerosol scale height, surface temperature and pressure. The individual retrieval steps are detailed in the following sections.

### *3.2.1 Cloud screening*

Artificial neural networks developed at FUB are used to perform the screening of clouds in MERIS L1B data, making use of the full set of spectral MERIS bands between 412nm and 900nm. The screening is done separately over ocean, land and ice/snow. In order to exclude cloud edges, a region of two pixels around each pixel classified as cloudy is screened as well.

Generally, cloud screening with MERIS is difficult due to the fact that no measurements in the thermal infrared spectral region are available, hampering the already hard detection of optically thin cirrus clouds. An underestimation of TCWV is to be expected where the cloud screening procedure fails to detect clouds.

### *3.2.2 Transmittance correction*

In the near infrared spectral range, the remotely sensable information about TCWV is the water vapour transmittance along the light path. Due to the spectral distance of MERIS bands 14 and 15, mainly noticeable through differences in surface reflectance and solar incoming irradiance, and the influence of atmospheric scattering, the measured band ratio $R_M = L_{15}/L_{14}$ deviates from the actual water vapour transmittance. The deviation is a function of the surface albedo and its spectral dependency, the viewing and illumination geometry and the vertical distribution and optical properties of the atmospheric scatterers. In a first step, the measured band ratio $R_M$ is therefore normalized by the ratio of the solar incoming irradiance $E_i$ at the particular wavelengths of both channels: $R_{M^*} = L_{15}/L_{14} * E_{14}/E_{15}$, taking into account the spectral smile effect, causing the central wavelength of MERIS bands to depend slightly on the viewing angle

(e.g. [RD-13]; [RD-14]). Afterwards, $R_{M^*}$ is simulated by the ratio of the water vapour transmittance in both bands, corrected for the spectral surface albedo difference and scattering processes in the atmosphere:
A fast forward model of the normalized band ratio $R_{M^*}$ as a function of TCWV, the viewing geometry, and the surface albedo, temperature and pressure is needed for the optimization of TCWV. It is based on pre-calculated absorption coefficients using an advanced k-distribution method [RD-10]). For a given amount of water vapour, the transmittance $T_j$ in MERIS band $j$ is modelled by accordingly adjusting the tabulated optical thickness $k_{ij}$, as it was calculated for fixed values of TCWV, calculating the transmittance for each of the $j$ k-bins following the Beer-Lambert law and summing up all transmittance values with respect to the weights $w_{ij}$ associated to the particular absorption bins:

$$T_j = \sum_{i=0}^{nbin} w_{ij} exp(-k_{ij}/\mu)$$

The k-coefficients are stored in look-up tables for 6 different temperature profiles ([RD-9]) and 27 different pressure levels. In order to account for the temperature- and pressure-dependence of the absorption lines, the transmittance is calculated for the four look-up table grid points closest to the actual surface pressure and temperature of the considered scene, hereby assuming that the surface temperature is highly correlated with the actual vertical temperature profile. The final transmittances of MERIS bands 14 and 15 are then calculated as a weighted average among these 4 figures.

As a next step, for land scenes the transmittance ratio is corrected for the difference in spectral surface reflectance. As the true surface reflectance at the MERIS wavelengths is unknown, it is estimated by correcting the measured reflectance at the top of the atmosphere for the scattering component, using a look-up table approach for the atmospheric correction. As this procedure is possible only in window channels, the surface albedo at 900nm is linearly extrapolated from $\alpha_{865nm}$ and $\alpha_{885nm}$, derived from the reflectances in MERIS bands 13 and 14. The atmospheric correction relies on information about the aerosol loading, type and vertical distribution. However, about the relatively bright land surfaces the influence on the surface reflectance retrieval is small, at least if absolute accuracy is not an issue but the primary goal is to determine the spectral slope in surface reflectance between the closely spaced MERIS bands. The albedo retrieval over land can thus be performed using climatological average values in case there is no additional information available.

Above the dark ocean the situation is different as there is no spectral dependency of the surface reflectance, however, the influence of atmospheric scattering on the measured band ratio is much more pronounced. Here, the surface reflectance can be simulated using the wind speed for parameterising the sea surface roughness ([RD-12], [RD-16]). In case of lacking background information about aerosols, the difference between calculated and observed reflectance is used to constrain the aerosol properties.

Finally, in order to correct the simulated transmittance ratio for the influence of atmospheric scattering, a scattering correction factor $f$ is extracted from tabulated MOMO simulations ([RD-7], [RD-8]). $f$ represents the relation between pure transmittance $T_{noscat}$, assuming a non-scattering atmosphere, and the true transmittance $T$, calculated with a full radiative transfer including multiple scattering events: $f = T/T_{noscat}$. Except for very high surface reflectance cases, $f$ is larger than one, as atmospheric scattering through reflection of incoming solar radiation altogether causes a shortening of the average photon path length in the atmosphere and reduces the amount of water vapour along the photon path by preventing a fraction of photons from traversing the

humid boundary layer. Figure 3 shows *f* and the equivalent error in retrieved TCWV when scattering is neglected as a function of Lambertian surface albedo and aerosol optical thickness for a total columnar water vapour of 56mm, a viewing zenith angle (VZA) of 30°, a solar zenith angle (SZA) of 64°, a relative azimuth angle (RAA) of 0° (≡ sensor is placed opposite of sun). The upper panels represent cases of boundary layer aerosols, whereas the lower panels belong to cases of highly elevated aerosol layers.

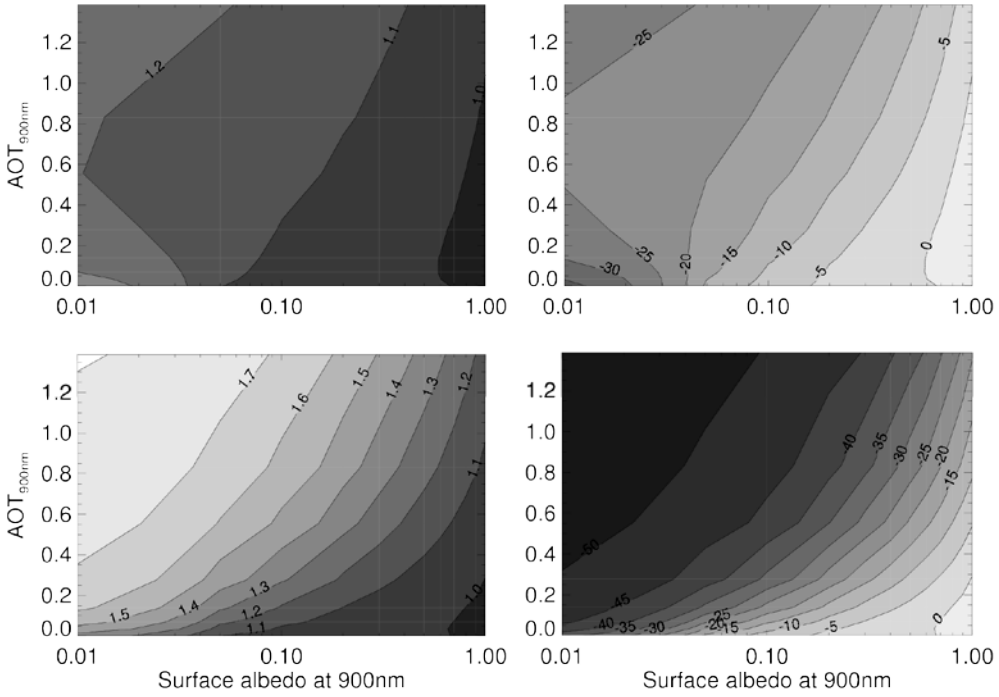


**Figure 3: Scattering correction factor *f* depending on surface albedo and aerosol optical thickness at 900nm (left panels) and equivalent underestimation of TCWV in mm when scattering is neglected (right panels), shown for SZA=64°, VZA=30°, RAA = 0°, TCWV = 56mm and a boundary layer (upper panels) and upper troposphere aerosol layer (lower panels).**

Several conclusions can be drawn from Figure 3:

1. As expected, the scattering correction factor is close to 1 for bright surfaces because the measured band ratio is dominated by photons that have been reflected at the bottom of the atmosphere.
2. Above dark surfaces such as the ocean, *f* is increased, as the predominant part of the detected photons is reflected by atmospheric scatterers and thus does not traverse the whole vertical column of water vapour.
3. Correspondingly, there is a strong bias in retrieved TCWV if scattering is neglected above dark surfaces and a less pronounced effect for bright surfaces.
4. Elevated aerosol layers (bottom panels) have a much stronger effect on the measured transmittance as compared to scatterers located in the boundary layer (upper panels).

The determination of the scattering factor f over an ocean surface distinguishes between surfaces with high (glint area) and low surface reflectance (off-glint area).

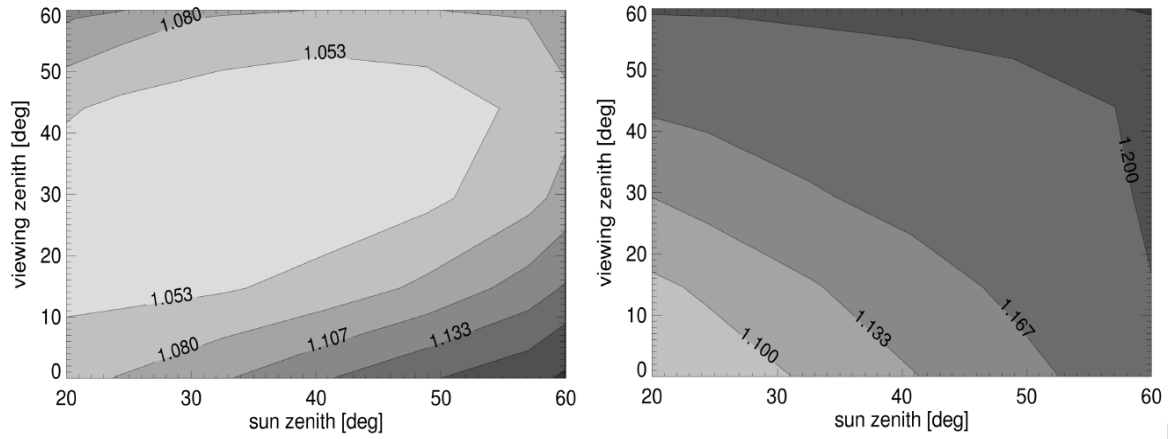


**Figure 4: Scattering correction factor f for the transmisson of MERIS-channel above an ocean surface as function of viewing- and sunzenith angle (low aerosol, AOT=0.35, windspeed=8 m/s, TCWV=42mm) left panel: RAA=0° (glint), right Panel: RAA=180° (off-glint)**

On the one hand, the influence of scattering on aerosols is bigger over dark areas (off-glint) than over bright areas (glint) (see figure 4). On the other hand, the determination of the aerosol optical depth is possible over dark surfaces but very uncertain over glint regions. Thus, the aerosol optical depth over the dark ocean surfaces is determined from the difference between calculated and observed reflectance, over bright surfaces the climatological mean value is used.

The surface reflectance for a given pixel is estimated analytically [RD-19] for the case-selection. The wind speed is taken reanalysis data or ECMWF.

Figure 5 shows global histograms of land surface albedo at 900nm throughout the year 2004, as extracted from the MERIS Albedomap ([RD-11]), providing 16-day averages of surface albedo in the MERIS bands on a 0.05° x 0.05° longitude-latitude grid.

In the near infrared spectral region the land surface reflectance is commonly larger than 0.2. In case of boundary layer aerosols, this corresponds to a bias of 10 - 30% in TCWV if scattering is neglected. For a dark ocean surface, the bias is in the range of 50%. In the less common case of highly elevated aerosols, these values are significantly higher. By applying the scattering correction factor to the modelled transmittance, the bias in retrieved TCWV is eliminated.

However, due to uncertainties in auxiliary parameters such as the surface reflectance and the prevailing aerosol type, optical thickness and vertical distribution, a residual uncertainty remains.

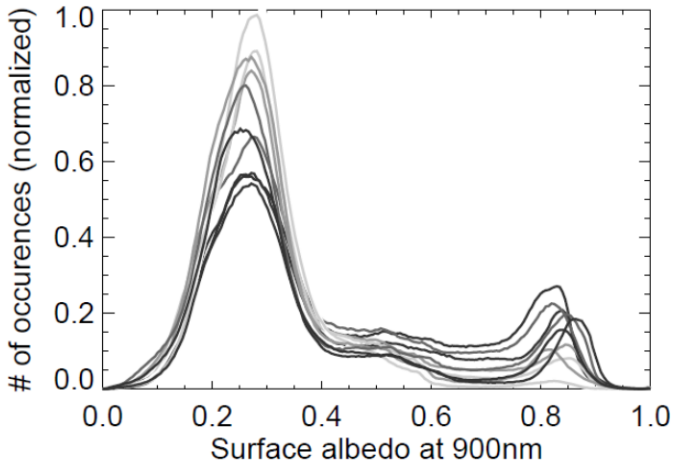


**Figure 5: Global, normalized histograms of surface reflectance at 900nm through the year 2004 (grey shading indicating seasonal dependence from winter (dark grey) to summer months (light grey). Extracted from the MERIS Albedomap.**

Due to the significantly stronger influence of scattering above dark surfaces, the resulting uncertainty of the derived water vapour column is much higher above the ocean. Over dark ocean areas (TOA reflectance < 0.1), the true ocean surface reflectance is calculated from the wind speed and the observing geometry ([RD-12], [RD-16]). The difference between TOA reflectance and calculated ocean surface reflectance is then used to estimate the aerosol loading and hereupon calculate the scattering correction factor *f*. This procedure is neither possible nor necessary when the sensor is directed towards the direct glitter of the sun, where the influence of the scattering atmosphere is weak and a climatological value of aerosol optical thickness can be used for the calculation of *f*.

### *3.2.3 Inversion technique*

In the retrieval scheme the first guess of TCWV is obtained from a simple regression, relating TCWV to a third order polynomial of $ln(L_{15}/L_{14})$, where the regression coefficients were determined using radiative transfer simulations with MOMO. In the iterative optimization routine, there is a single variable to bet fitted, the total columnar water vapour, using a single piece of information, the MERIS band ratio $R = L_{15}/L_{14}$, with a monotonic relation between both figures. The use of background information about TCWV such as e.g. NWP reanalysis data is therefore not necessary, as it only dilutes the high sensitivity inherent to the MERIS measurement. The straightforward optimization of TCWV is performed by the secant method. It was preferred to the Newton method in spite of its slightly slower convergence, because there is no need to calculate the derivative of the cost function at every retrieval step, so its implementation provides a faster processing in practice. Starting with the first guess, TCWV is adjusted until the cost function, represented by the absolute difference between simulated and measured ratio of normalized radiances in MERIS bands 15 and 14, is below a pre-defined threshold, determined by e.g. the sensor noise.

### *3.2.4 Uncertainty estimate*

Once the iteration procedure has converged the retrieval uncertainty is calculated, taking into account direct measurement errors, that is instrumental noise, as well as the uncertainties of all those parameters that are not part of the state vector but are fixed a priori. These are the surface albedo and its spectral dependency, the temperature profile, the surface pressure, the aerosol optical thickness and the aerosol height. The uncertainty introduced by these modelling parameters $b_i$ is determined by converting the individual error contributions into measurement space via the modelling parameter Jacobian $K_b$ and adding them to the measurement error covariance matrix $S\varepsilon$, which in our case is just a scalar, as we are only using one piece of information, namely the band ratio $R$:

$$S_y = S_\varepsilon + K_b^T S_b K_b$$

The resulting error covariance matrix $S_y$, again in our case just a scalar variance of $R$ due to all measurement and model parameter uncertainties, is converted into parameter space using the Jacobian $K$, that is the partial derivative of the band ratio $R$ with respect to TCWV at the retrieved state. As a result we get $\hat{S}$, the variance of the retrieved state, that is directly used to define the measurement uncertainty (as detailed in [RD-15]):

$$\hat{S} = (K^T S_y^{-1} K)^{-1}$$

In particular, the uncertainties of the individual parameters are estimated as follows. As detailed in section 3.2.2, among the above parameters there are 3 candidates affecting the scattering correction factor $f$, namely the absolute surface reflectance, the aerosol optical thickness and the aerosol height. For each of these parameters, an $f^*_i$ (with i = 1;2;3) is calculated from the look-up tables, by perturbing the input accordingly. The perturbance value is 0.1 in case of aerosol optical thickness and 0.02 for the surface albedo. Since there is no information about the vertical distribution of the aerosols, a large error is assumed by shifting the aerosol layer to the high troposphere instead of locating it in the boundary layer. Instead of $f$, the $f^*_i$ are used to correct the simulated transmittance for scattering, in each case resulting in a perturbed band ratio $R^*_i$. We obtain the deviation of the modelled band ratio $\Delta R_i = |R^*_i - R|$ for each of the three parameters.

In case of surface pressure and temperature, the forward model is used directly to simulate perturbed transmittances that are corrected with an unperturbed scattering correction factor $f$. The assumed uncertainties are 10hPa for surface pressure and 5K for the surface temperature, respectively.

Above land, the uncertainty introduced by the spectral albedo slope is parameterised with the normalized differenced vegetation index (NDVI) of the observed scene. As shown in Figure 6, the linear extrapolation of $\alpha_{865nm}$ and $\alpha_{885nm}$ towards 900nm is a good approximation for vegetated surfaces with an NDVI around 0.6 and less accurate for e.g. bare soils or snow covered areas. Therefore, the NDVI is used to estimate the uncertainty introduced, ranging from 0.001 to 0.003 for snow-free areas up to 0.006 above snow and ice. As there is no spectral albedo slope above ocean, no error contribution is calculated here. Further, if the reflectance at channel 14 is below 0.05 the uncertainty estimation is not valid and the uncertainty is set to 0.

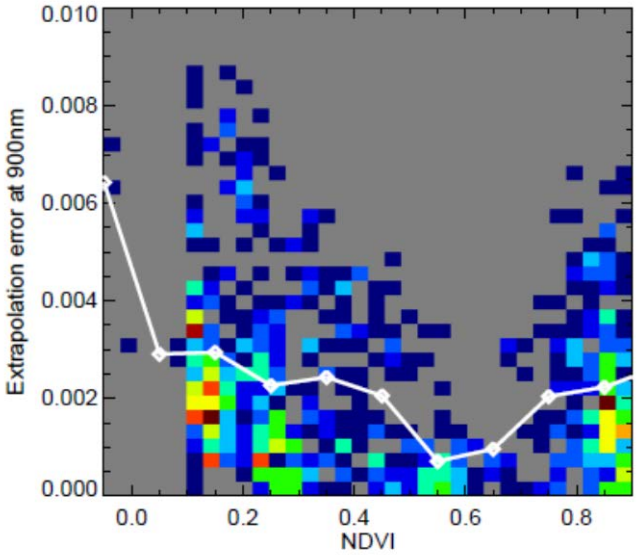


**Figure 6: Normalized frequency of occurrence of error of linearly extrapolated surface albedo at 900nm, depending on NDVI and resulting error parameterisation (white curve).**

The final contribution to the retrieval uncertainty is the sensor noise with an assumed signal-to-noise-ratio of 250. The resulting overall uncertainty of the retrieved TCWV is large over dark targets, where the unknown aerosol vertical distribution is the predominant contributor to the retrieval uncertainty. Over non-vegetated land areas and especially ice and snow-covered regions, an important error contribution is the spectral albedo slope uncertainty.

# 4 Assumptions and limitations

Due to the dominating influence of atmospheric scattering, above ocean a reduced accuracy of the MERIS-derived TCWV is to be expected.

Generally, the quality of the MERIS TCWV retrieval algorithm strongly depends on the reliability of the cloud screening procedure used. Since MERIS does not provide measurements in the thermal infrared, the screening of optically thin cirrus clouds is difficult. A weak dry bias is to be expected, where the cloud detection fails to detect cirrus clouds.

Since the MERIS retrieval is only applied for clear sky scenes, any derived higher-level products, such as monthly means, are clear-sky only products. A clear-sky bias can be expected when comparing MERIS-derived statistics against other data sets, when cloudy cases are not properly filtered out in the reference data set.

Among the errors sources of the retrieval is the uncertainty of the water vapour continuum absorption. Recent publications, such as [RD-17], have shown that the strength of the continuum absorption throughout the spectrum is still highly uncertain. Instead of cutting the absorption lines close the centre and adding a background continuum absorption to account for the overlapping line wings, the line wings were not cut off at all and consequently no continuum was added. Validation exercises have shown that the bias of the resulting product is well within the uncertainty of the gas absorption.

# 5 Conclusions

The MERIS L2 algorithm used for the TCWV retrieval is described in detail in this document. The retrieval is based on the exploitation of the differential absorption of water vapour in the near infrared, as measured by MERIS bands 14 and 15. The algorithm builds on previous developments at FUB and provides the total columnar water vapour over cloud free land and ocean during daytime. Validation results over land and ocean can be found in [RD-18].

The forward operator used in the retrieval algorithm is a simple model of the water vapour transmittance in the MERIS bands. The calculated transmittance ratio is corrected for the influence of scattering in the atmosphere, using pre-calculated look-up tables of correction factors. These look-up tables were calculated using the full radiative transfer code MOMO. Realistic uncertainty estimates are provided on a pixel-by-pixel basis, by taking into account all relevant sources of uncertainty, such as sensor noise and, more important, errors of forward